Inverted Scanning Microwave Microscopy of GaN/AlN High-Electron Mobility Transistors

Xiaopeng Wang[1], Kazuki Nomoto[1], Gianluca Fabi[1], Richard Al Hadi[2], Marco Farina[3], Debdeep Jena[1], Huili Grace Xing[1], James C. M. Hwang[1]

[1]Cornell University, Ithaca, NY, USA
[2]Ecole de Technology Superior, Montréal, QC, Canada
[3]Marche Polytechnic University, Ancona, Italy

2024 103rd ARFTG Microwave Measurement Conference (ARFTG) | 979-8-3503-6273-2/24/$31.00 ©2024 IEEE | DOI: 10.1109/ARFTG61196.2024.10660702

***Abstract* — In this paper, an inverted scanning microwave microscope (iSMM) is used to characterize the channel of a gate-less GaN/AlN high-electron-mobility transistor (HEMT). Unlike conventional SMM, iSMM allows for 2-port measurements. Unlike conventional iSMM, the present iSMM probe is connected to Port 1 of a vector network analyzer with the HEMT drain and source remain on Port 2. Under different DC biases V_{GS} (applied through the iSMM probe) and V_{DS} (kept constant at 1 V), changes in both reflection coefficient S_{11} and transmission coefficient S_{21} are monitored as the iSMM probe scans along the width of the channel, revealing significant nonuniformity. Additionally, changes in S_{11} and S_{21} are significant when $V_{GS} \geq -4$ V, but insignificant when $V_{GS} = -8$ V, consistent with the measured threshold voltage at −6 V for a gated HEMT. These results confirm that iSMM can be used to locally modulate the channel conduction of a HEMT while monitoring its RF response, before the actual gate is added. In turn, the nonuniformity measured by the iSMM can be used to diagnose and improve HEMT materials and processes.**

***Index Terms* — Scanning microwave microscope, transfer characteristics, two-dimensional electron gas, GaN HEMT**

I. Introduction

The scanning microwave microscope (SMM) has been proven to be a useful metrology tool for semiconductor characterization and biological imaging [1]–[5]. The raster scan controlled by the feedback of force as in an atomic force microscopy (AFM) affords SMM nanometer vertical resolution and sub-micrometer lateral resolution. The microwave signal injected through the SMM probe allows it to analyze the electromagnetic properties of the sample from the reflected signal. The microwave signal penetrates into the sample on the order of micrometer to characterize layers below the surface.

Recently, an inverted SMM (iSMM) has been developed to improve the dynamic range, bandwidth, and robustness of SMM [6]. The improvements by the iSMM have been shown in characterization of biological cells and 2D atomic layers [6], [7]. Unlike conventional SMM, the iSMM allows 2-port measurements in which the SMM probe is grounded while scanning over a sample mounted on a transmission line with its input and output connected to Port 1 and Port 2, respectively, of a vector network analyzer (VNA). To evaluate the possibility of further improvement to 3-port measurements, in this paper, the iSMM probe is connected to Port 1 of the VNA while scanning over an *ungated* GaN/AlN high-electron-mobility transistor (HEMT) [8]. The drain remains connected to Port 2. To modulate the HEMT channel, in lieu of an actual gate, a DC bias is superimposed on the iSMM probe as in conventional SMM [9], [10] and detailed below.

II. Experimental

Fig. 1 illustrates the iSMM based on a Keysight Technologies 7500 AFM equipped with an N9545C SMM nose cone and a Rocky Mountain 25Pt300A platinum probe with a spring constant of 18 N/m. The probe is affixed to a cantilever with its deflection monitored by a laser. The cantilever, in turn, is connected to Port 1 of a Keysight Technologies E8062B VNA through a coaxial cable. The cable is shunted by a 50-Ω resistor for impedance matching around 3 GHz and its harmonics. Fig. 2(a) is a photograph of the iSMM with its sample chamber open to show the sample holder mounted on the ceiling of with three cables connected to the source, gate and drain of the ungated GaN/AlN HEMT. Fig. 3 shows the details of the HEMT mounted on a printed circuit board (PCB) and, in turn, the sample holder. The drain is connected to Port 2 through a bond wire, a PCB via, an SMA connector on the PCB bottom, and a coaxial cable. The source is grounded.

The VNA generates on Port 1 a 0-dBm signal at 12.97 GHz. Following near-field interaction with the sample, the reflection coefficient S_{11} and the transmission coefficient S_{21} are measured on Port 1 and Port 2, respectively, while the AFM topography is simultaneously recorded. The intermediate frequency bandwidth is set at 500 Hz as a compromise between the scan rate and the signal-to-noise ratio (SNR). With a scan rate of 16 pixel/s, it takes approximately 5 min to scan a 2 μm × 32 μm area with a resolution of 16 × 256 pixels. A Keysight E3620A dual DC power supply provides the gate-source bias V_{GS} to the HEMT via a Keysight 11612A bias-T on Port 1 and the drain-source bias V_{DS} via an internal bias-T built in the VNA on Port 2.

Fig. 2(b) illustrates the sample structure grown by Veeco using metal-organic chemical vapor deposition on 700-μm 3-kΩ·cm Si. It can be seen that the structure consists of sequentially grown layers, starting with a 100-nm AlN nucleation layer, followed by a 500-nm AlGaN

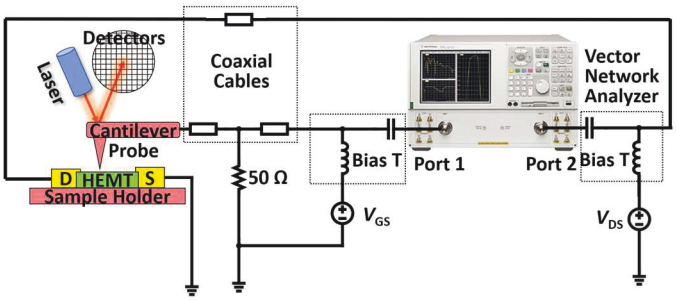

Fig. 1. Schematic of the present iSMM setup.

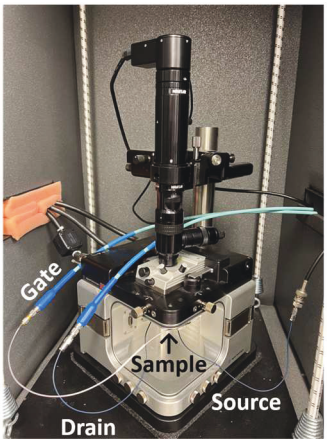

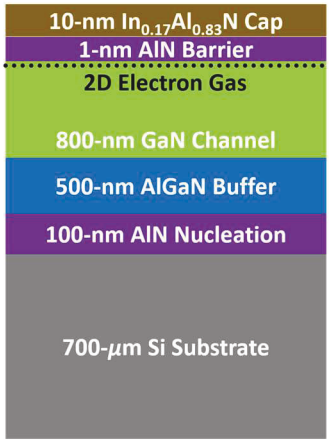

Fig. 2. (a) Photograph of the iSMM with its sample chamber open. (b) Sample layer structure.

buffer layer, an 800-nm GaN channel layer, a 1-nm AlN barrier layer, and, finally, a 10-nm $In_{0.17}Al_{0.83}N$ cap layer. Thus, the channel conduction is through a two-dimensional electron gas at the GaN/AlN heterojunction 11 nm below the surface except where it is isolated by dry etching to a depth of 170 nm.

III. Results and Discussion

A. AFM Topography and DC Current-Voltage Characteristics

Fig. 4(a) shows the AFM image of the channel of the *ungated* HEMT. It can be seen that the channel is approximately 2.5-μm long and 24-μm wide. Because the radius of the iSMM probe tip is approximately 0.5 μm, the scan length from the source to the drain is limited to 2 μm. On the other hand, the scan width is purposely made larger than 24 μm, so that the measure data outside the channel can be used as a reference. Fig. 4(b) shows the AFM line scan across the middle of the channel halfway between the source and drain. It confirms that the etch depth is approximately 170 μm outside the channel.

Fig. 5 shows the DC-measured transfer and output characteristics of a *gated* HEMT on the same chip as the *ungated* HEMT. It can be seen that the threshold voltage $V_{TH} \approx -6$ V.

B. Reflection Coefficients Measured by iSMM

Fig. 6 shows the iSMM images and line scans of changes in

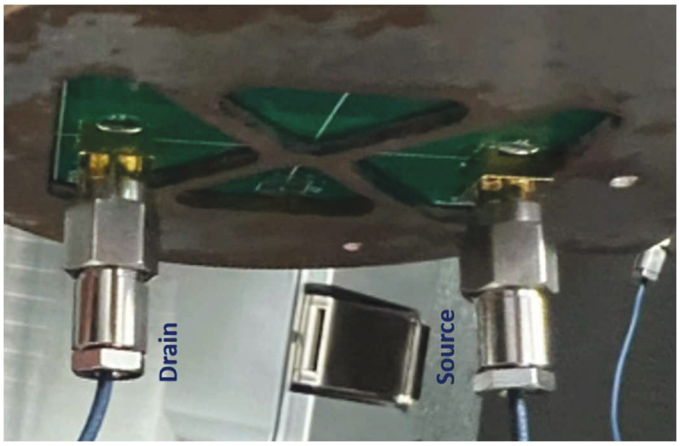

(a)

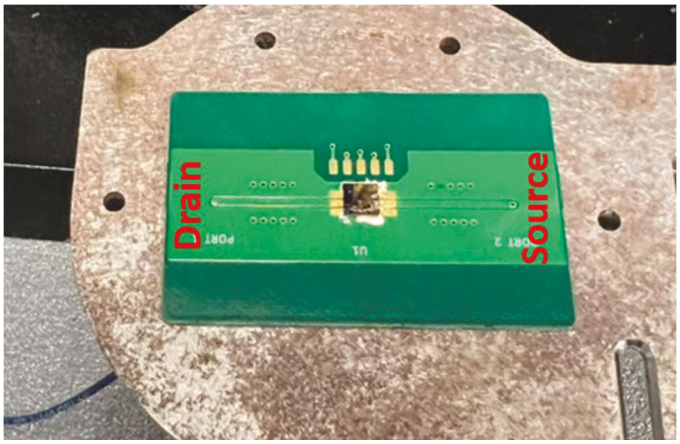

(b)

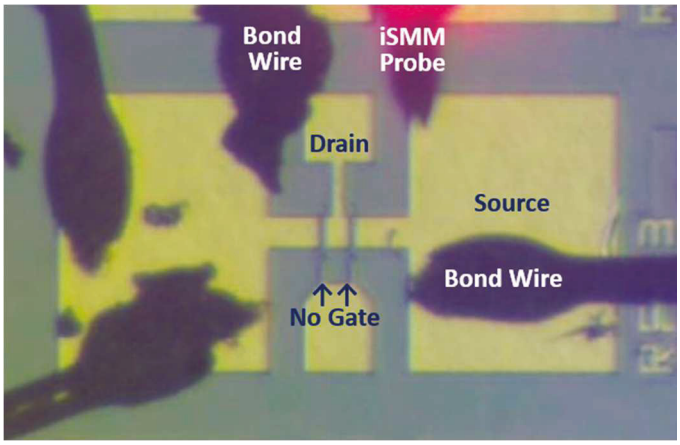

(c)

Fig. 3. (a) Source and drain cables connected to the PCB bottom via SMA connectors. (b) The PCB top with the HEMT chip mounted in the middle and its source and drain wire-bonded to two coplanar transmission lines each terminating in a via. (c) The HEMT with two parallel channels and two sources. The left source is shorted to the drain by a bond wire, while the right source is grounded. The right channel is scanned by the iSMM probe.

the magnitude and phase of the reflection coefficient, $\Delta|S_{11}|^2$ and $\Delta\angle S_{11}$, respectively, with respect to the average outside the

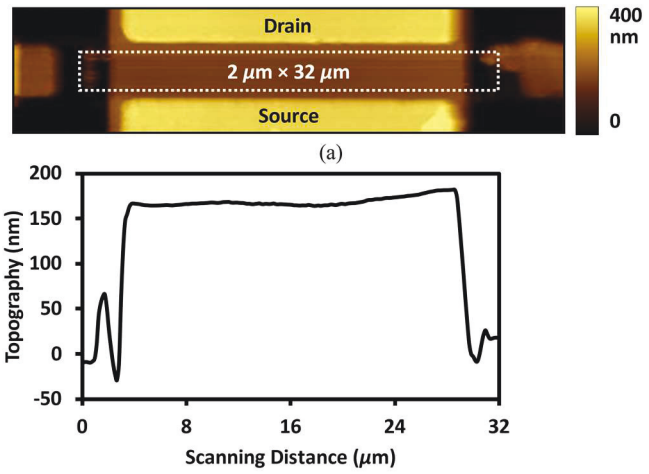

Fig. 4. (a) AFM image of the channel of an *ungated* HEMT. (b) AFM line scan across the middle of the channel halfway between the source and drain.

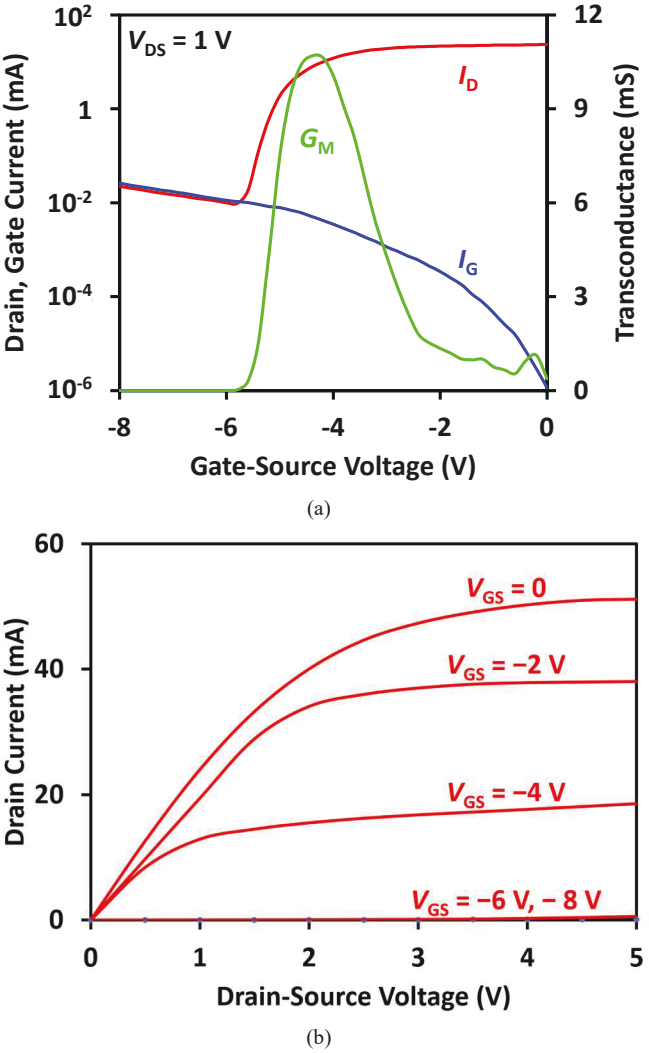

Fig. 5. DC (a) transfer and (b) output characteristics of a *gated* HEMT.

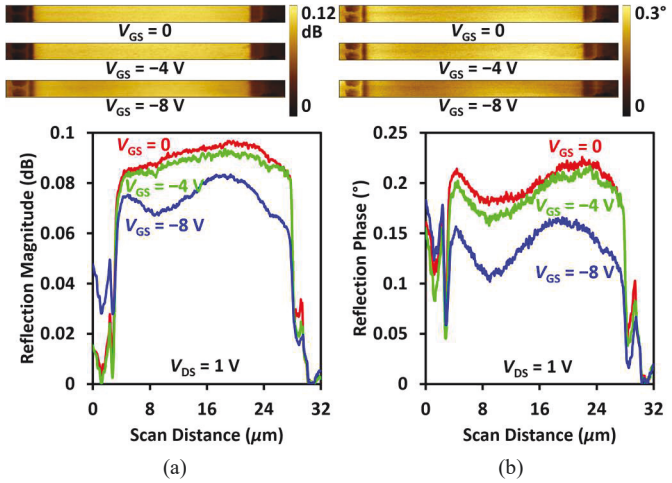

Fig. 6. Images and line scans by iSMM of changes in (a) magnitude and (b) phase of the reflection coefficient under different gate biases.

channel. V_{DS} = 1 V. With V_{GS} = 0 or −4, finite changes can be seen so that $\Delta|S_{11}|^2 \approx 0.1$ dB and $\Delta\angle S_{11} \approx 0.2°$. However, with V_{GS} = −8 V, changes reduce to $\Delta|S_{11}|^2 \approx 0.07$ dB and $\Delta\angle S_{11} \approx 0.1°$, indicating that the channel is depleted which is consistent with $V_{TH} \approx -6$ V of the gated HEMT. From the iSMM line scans, it can also be seen that the channel is non-uniform across its width with the left side generally lower than the right side. Since the DC measurement of a gated HEMT only gives the total current across the entire width of the channel, the detailed variation revealed by iSMM can help diagnose material or process problems.

C. Transmission Coefficients Measured by iSMM

Fig. 7 shows the iSMM images and line scans of changes in the magnitude and phase of the transmission coefficient, $\Delta|S_{21}|^2$ and $\Delta\angle S_{21}$, respectively, with respect to the average outside the channel. V_{DS} = 1 V. In general, changes in S_{21} are not as prominent as in S_{11}, but the same trend is discernable. With V_{GS} = 0 or −4, $\Delta|S_{21}|^2 \approx 0.03$ dB. With V_{GS} = −8 V, changes reduce to $\Delta|S_{11}|^2 \approx 0.015$ dB, again indicating that the channel is depleted. In all cases, $\Delta\angle S_{11} \approx 0.04°$, probably due to topography crosstalk instead of channel conduction [11]. Nonuniformity across the channel width is also observed, but not as obvious as in S_{11}.

From the above, $\Delta|S_{11}|^2$ and $\Delta\angle S_{11}$ appear to have higher sensitivity and SNR than $\Delta|S_{21}|^2$ and $\Delta\angle S_{21}$ have, which is opposite to our previous observation with the iSMM probe grounded [6], [7]. This is because in the present case the HEMT is better matched in the input than the output. In particular, the HEMT drain is connected to Port 2 via a millimeter-long bond wire with a large associated inductance. Consequently, $|S_{21}|^2$ is on the order of −50 dB, resulting in low sensitivity and SNR. In the future, better iSMM sensitivity and SNR in both S_{11} and S_{11} can be expected with improved input and output impedance matching.

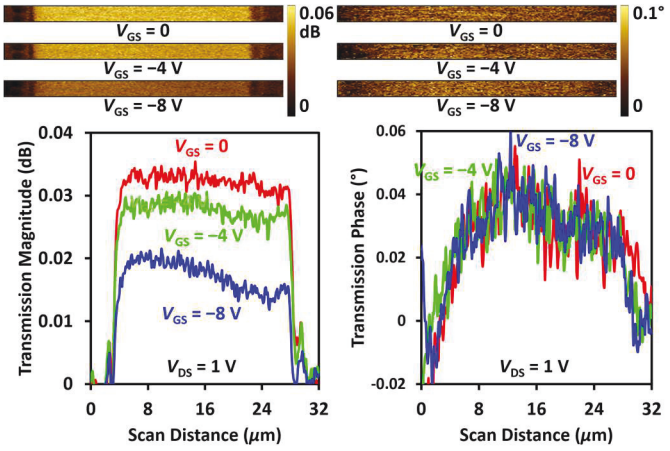

Fig. 7. Images and line scans by iSMM of changes in (a) magnitude and (b) phase of the transmission coefficient under different gate biases.

IV. Conclusion

This study investigates the use of an iSMM for in-process characterization of the GaN/AlN heterostructure. The iSMM-measured reflection and transmission coefficients are effective in detecting variations in conduction through the heterostructure. The detected variations are consistent with current-voltage characteristics measured after the heterostructure is gated and turned into a HEMT. The iSMM detects nonuniformity across the width of the channel which can help diagnose material or process problems. With the success in connecting the iSMM probe to the VNA for both stimulating and sensing microwave signals, in the future, the iSMM can be configured in 3 ports for more complicated but informative measurements such as intermodulation measurements.

Acknowledgement

This work was supported in part by the Semiconductor Research Corporation and the US Defense Advanced Research Projects Agency through the Joint University Microelectronics Program, the US Army Grants W911NF-14-1-0665, W911NF-17-1-0090, W911NF-17-P-0073, W911NF-18-C-0094, and W911NF-24-1-0023, the US Air Force under Grants FA9550-16-1-0475, FA9550-17-1-0043, and FA9550-20-1-0148, the US National Science Foundation (NFF) under Grants 1433459-EFMA, 1710298-DMR, 2117305-ECCS, and 2132323-ECCS. Devices are fabricated in the Cornell NanoScale Facility, an NNCI member supported by NSF Grant NNCI-2025233. Material characterization is aided by the Cornell Center for Materials Research supported by the NSF MRSEC program (Grant 1719875-DMR). This work is also supported by ARFTG student fellowship.

References

[1] R. C. Chintala, K. Rubin, and Y. Yang, "Scanning microwave impedance microscopy: Room-temperature and low-temperature applications for device and material characterization," *IEEE Microw. Mag.*, vol. 21, no. 10, pp. 22–35, Oct. 2020.

[2] S. Berweger, T. M. Wallis, and P. Kabos, "Nanoelectronic characterization: Using near-field microwave microscopy for nanotechnological research," *IEEE Microw. Mag.*, vol. 21, no. 10, pp. 36–51, Oct. 2020.

[3] M. Farina and J. C. M. Hwang, "Scanning microwave microscopy for biological applications: Introducing the state of the art and inverted SMM," *IEEE Microw. Mag.*, vol. 21, no. 10, pp. 52–59, Oct. 2020.

[4] L. Zheng, L. Shao, M. Loncar, and K. Lai, "Imaging acoustic waves by microwave microscopy: Microwave impedance microscopy for visualizing gigahertz acoustic waves," *IEEE Microw. Mag.*, vol. 21, no. 10, pp. 60–71, Oct. 2020.

[5] A. Tselev, "Near-field microwave microscopy: Subsurface imaging for in situ characterization," *IEEE Microw. Mag.*, vol. 21, no. 10, pp. 72–86, Oct. 2020.

[6] M. Farina, X. Jin, G. Fabi, E. Pavoni, A. D. Donato, D. Mencarelli, A. Morini, F. Piacenza, R. A. Hadi, Y. Zhao, Y. Ning, T. Pietrangelo, X. Cheng, and J. C. M. Hwang, "Inverted scanning microwave microscope for in vitro imaging and characterization of biological cells," *Appl. Phys. Lett.*, vol. 114, no. 9, p. 093703, Mar. 2019.

[7] G. Fabi, X. Jin, E. Pavoni, C. H. Joseph, A. D. Donato, D. Mencarelli, X. Wang, R. A. Hadi, A. Morini, J. C. M. Hwang, and M. Farina, "Quantitative characterization of platinum diselenide electrical conductivity with an inverted scanning microwave microscope," *IEEE Trans. Microw. Theory Techn.,* vol. 69, no. 7, pp. 3348–3359, Jul. 2021.

[8] L. Li, K. Nomoto, M. Pan, W. Li, A. Hickman, J. Miller, K. Lee, Z. Hu, S. J. Bader, S. M. Lee, J. C. M. Hwang, D. Jena, and H. G. Xing, "GaN HEMTs on Si with regrown contacts and cutoff/maximum oscillation frequencies of 250/204 GHz," *IEEE Electron Device Lett.*, vol. 41, no. 5, pp. 689–692, May 2020.

[9] D. Wu, X. Li, L. Luan, X. Wu, W. Li, M. N. Yogeesh, R. Ghosh, Z. Chu, D. Akinwande, Q. Niu, and K. Lai, "Uncovering edge states and electrical inhomogeneity in MoS_2 field-effect transistors," *Proc. Natl. Acad. Sci. U.S.A.*, vol. 113, no. 31, pp. 8583–8588, Aug. 2016.

[10] S. Berweger, J. C. Weber, J. John, J. M. Velazquez, A. Pieterick, N. A. Sanford, A. V. Davydov, B. Brunschwig, N. S. Lewis, T. M. Wallis, and P. Kabos, "Microwave near-field imaging of two-dimensional semiconductors," *Nano Lett.*, vol. 15, no. 2, pp. 1122–1127, Feb. 2015.

[11] G. Fabi, C. H. Joseph, E. Pavoni, X. Wang, R. A. Hadi, J. C. M. Hwang, A. Morini, and M. Farina, "Real-time removal of topographic artifacts in scanning microwave microscopy," *IEEE Trans. Microw. Theory Techn.*, vol. 69, no. 5, pp. 2662–2672, May 2021.